Enhancement of optical and electrical properties of spray pyrolysed ZnO thin films obtained from nitrate chemical by Al-Sn co-doping

K. Salim, M. Medles, A. Nakrela, R. Miloua, A. Bouzidi, Rachel Desfeux

Enhancement of optical and electrical properties of spray pyrolysed ZnO thin films obtained from Nitrate chemical by Al-Sn co-doping

K. Salim [a*], M. Medles [a], A. Nakrela [a], R. Miloua [a,b], A. Bouzidi [a], R. Desfeux [c]

[a] Laboratoire d'Elaboration et de Caractérisation des Matériaux, Département d'Electronique, Université Djillali Liabes, BP89, Sidi Bel Abbés 22000, Algeria

[b] Faculté des Sciences de la Nature et de la Vie, Université Ibn Khaldoun 14000 Tiaret, Algeria

[c] Univ. Artois, CNRS, Centrale Lille, ENSCL, Univ. Lille, UMR 8181, Unité de Catalyse et Chimie du Solide (UCCS), F-62300 Lens, France

Abstract

Un-doped, Al-doped, and Sn-Al co-doped ZnO thin films have been successfully synthesized by Spray Pyrolysis method. Zinc Nitrate ($Zn(NO_3)_2$), Tin Chloride ($SnCl_2$) and Aluminum Nitrate ($Al(NO_3)_3$) were used as starting chemicals at different compositions. Films depositions were carried out on glass substrates at 350°C. The X-ray diffraction confirmed that the Al-Sn co-doping did not change the ZnO Hexagonal Wurtzite structure. The obtained un-doped ZnO films were highly oriented along the preferential (002) crystallographic plane while the Sn- Al co-doped ZnO films were disoriented with slight loss of crystallinity. The optical measurement showed an increase of the average transmittance from 65 % to 81 % and the band gap energy (E_g) from 3.23 to 3.30 eV. The electrical conductivity has increased with the Al-Sn co-doping concentration to reach the value of 0.335 $(\Omega.cm)^{-1}$.

Keywords: ZnO; Al-Sn co-doping; thin films; Spray pyrolysis

Address of corresponding author:

Karim SALIM

Université Djillali Liabbès de Sidi Bel Abbès

Département D'Electronique

BP 89, Sidi Bel Abbès, 22000, Algérie.

Tél/Fax : 21348543018/21348563068

E-mail : karim22000@hotmail.com

1. Introduction

In recent years, zinc oxide (ZnO) has been of increasing interest in many research works because of its many potential applications. ZnO is a nontoxic (II-VI) binary semiconductor material [1] with very interesting characteristics such as piezoelectricity [2], photoconductivity [3], optical waveguides [4] and gas probes [5].

ZnO thin films can be obtained by several techniques such as pulsed laser deposition [6], thermal evaporation [7], sputtering [8], sol gel [9] and spray pyrolysis [10-14]. Among these techniques, spray pyrolysis remains attractive and interesting owing to its low cost, simplicity, rapidity, and also the possibility to make large area coatings.

Although, undoped ZnO thin films have been obtained with interesting electrical and optical properties [15-16] using spray pyrolysis and zinc acetate as starting chemicals, a great deal of work has been devoted to improve their properties by doping and co-doping. Currently, using zinc acetates with Sn an Al co-doping, the ZnO conductivity and transmittance values of the order of 10^{+2} $(\Omega.cm)^{-1}$ and 75%, respectively, have been reached.

Paradoxically, although thin ZnO films of good structural quality (i.e. highly oriented) were obtained from zinc nitrate using the spray technique, their conductivity and transparency remained unsatisfactory in the order of 10^{-3} $(\Omega.cm)^{-1}$ and 65%, respectively. The bibliography shows that the investigating studies about doping and co-doping ZnO thin films obtained from zinc nitrate had not had the amount required in order to improve them electrically and optically.

In this present study, by using the spray pyrolysis technique, zinc nitrate, tin chloride and aluminum nitrate have been used as starting chemicals to obtain the pure (undoped), aluminium doped and aluminum-tin co-doped ZnO thin films at different compositions. Structural, optical and electrical properties have been investigated to study the doping and co-doping effects on the obtained ZnO thin films.

2. Experimental details

The thin films of un-doped, Al-doped and Al-Sn co-doped ZnO were deposited by spray pyrolysis technique on amorphous glass substrates with dimensions of 75 × 25 mm^2. The glass substrates were cleaned by diluted hydrochloric acid and acetone, washed by double distilled water and dried. The sprayed solutions have been obtained by dissolving zinc nitrate ($Zn(NO_{3)2}.6H_2O$), aluminium nitrate ($Al(NO_3)_3.9H_2O$), and tin chloride ($SnCl_2.2H_2O$), in doubly distilled water with a concentration of 0.1 M.

The prepared solutions of zinc nitrate, aluminium nitrate and tin chloride were appropriately mixed to obtain the desired sprayed solutions of pure, Al-doped and Al-Sn co-doped ZnO. Tab.1 summarizes the sprayed solution compositions used to obtain the samples. The sample designations given in Tab.1 will be used in the discussion part.

For the spray pyrolysis system (Fig. 1) a compressed air at a pressure of 6×10^4 Pa has been used as a carrier gas. In the samples preparation process, the following conditions have been considered: substrate temperature 350 ± 10°C, solution flow of 2 ml /min and spray nozzle to heating plate distance of 30 cm. A mixed solution volume of 50 ml has been used for each sample composition. In order to avoid excessive cooling of the glass substrates resulting from continuous spray, two minute intervals of time have been taken between spraying periods. One also notes that the prepared solutions were immediately sprayed to avoid any possible chemical changes with time.

The structural characterization was performed at room temperature using a Bruker X-ray diffractometer model D2 Phaser with CuKα radiation ($\lambda = 1.5406$ Å). The analyses of surface morphology and chemical composition were carried out using a Jeol JSM 5800 scanning electron microscope which is equipped with energy dispersive X-ray detector (EDX, IXRF Model 550i). The optical transmittances have been recorded between 200 and 2500 nm wavelength using a JASCO 570 type UV-visible-NIR double-beam spectrophotometer. The electrical parameters were measured by using the ECOPIA HMS-5000 Hall Effect measurement system at room temperature. The XPS measurements were carried out on a Kratos Axis Ultra using Al K_α (1486.6 eV) radiation. High resolution spectra were acquired at 20 eV pass energy with energy resolution of 0.9 eV. The C1s line of 284.5 eV was used as a reference to correct the binding energies for charge energy shift. The surface topography of the deposited films were analyzed using the Dektak XT Stylus Profilometer, a good alternative to the Atomic Force Microscope for RMS (Root Mean Square) measurement on large areas.

3. Results and discussion

3.1 Structural properties and morphology

The structural features of un-doped, Al doped (AZO) and co-doped Al and Sn ZnO (ATZO) thin films have been analysed by XRD measurement. Fig. 2(a) shows the X-ray diffraction patterns of the obtained Al-Sn co-doped and un-doped ZnO films. For the co-doped samples, the concentration of Al is maintained at 1% however, the Sn concentration is varied from 0 to 1% according the experimental procedure mentioned previously. The value of the 1% Al doping

of ZnO thin films was set based on the work already done [13, 17] to improve both the electrical and optical properties. The results reported elsewhere [17] suggest that the Al doping limit of ZnO was 2% in the case of the spray pyrolysis technique.

The XRD spectra of the un-doped ZnO films were characterized by a strong peak at $2\theta = 34.521°$ which indicates a highly preferential orientation along [002] crystallographic plane. This result obtained by spray pyrolysis with aqueous solution of zinc nitrate was already achieved by the same technique [18], using zinc chloride and zinc acetate [19-22].

After doping, several peaks appeared in the XRD spectra of the ZnO films obtained. All these observed peak positions are in agreement with those of standard ZnO: JCPDS (Joint Committee of Powder Diffraction Standards) N° 36-1451. The spectra examination revealed no diffraction peaks attributed to Al or Sn neither to their oxides, suggesting that the films show no segregation or formation of secondary phases or coexisting phases, while confirming the success of the doping of the ZnO thin films.

As shown in Fig. 2(b), at 1% Al doping, ZnO films maintained a preferential orientation on the crystallographic plane [002] with a slight loss of crystallinity, as shown by the shift of the peak position (002) towards higher values of 2θ. This behavior remains the same as long as the doping level in Al is below 1% as shown elsewhere [13]. In fact, it was shown that below of the amount of 1% Al added, the Al atoms are located on the substitution sites and the interstitial occupation is ruled out [13].

On the other hand, starting of the increase of the peaks (100) and (101) noticed on XRD spectra shows the beginning of random orientation. This random orientation of AZO films has been accentuated by Sn incorporation in addition to Al (samples ATZO-0.25, ATZO-0.5, ATZO-0.75 and ATZO-1), which has been noticed by the progressive increase of (100) and (101) peaks, and the decrease of (002) one.

In order to explore this XRD spectra evolution trend due to the incorporated foreign atoms, the grain sizes, lattice constants, strains and dislocation density have been evaluated according to Fig. 3. For the estimation of crystallite size the Sherrer formula is used [23]:

$$D = \frac{k\lambda}{\beta \cos\theta} \quad (1)$$

Where k = 0.9, λ = 1.5406 Å is the x-ray wavelength, β is the full width at half maximum (FWHM) of the XRD peak, and θ is Bragg's diffraction angle.

The lattice parameters of the films are determined by the following relation [24]:

$$\frac{1}{d^2{}_{hkl}} = \frac{4}{3}\left(\frac{h^2 + hk + k^2}{a^2}\right) + \left(\frac{l^2}{c^2}\right) \quad (2)$$

The micro-strain (ε) has been estimated using the following formula [25]:

$$\varepsilon = \frac{\beta \cos\theta}{4} \quad (3)$$

The dislocation density of the films has been estimated using the following formula **[**26]:

$$\delta = \frac{1}{D^2} \quad (4)$$

All the structural parameters, i.e. full width at half maximum (FWHM), crystallite sizes, lattice constants (a and c), strains and dislocation density are summarized in Tab. 2. According to Fig. 2(a), the crystallinity degradation is attributed to dopants introduction. The crystallite size decreases after doping (see Fig.3), which has already been observed by several authors [27-28].

On the other hand, the XRD spectra showed a small shift towards higher angle of the (002) peak position for Al doping at 1% concentration which imply a decreasing in lattice parameters (Tab. 2) and as result a compressive stress. When ZnO thin films are Al doped, similar shifts that are in agreement with our results have been also observed in several works [13, 17, 29] and predicted by First-Principles study of M. Wu *et al.*[30]. In the latter work, the authors explained this behavior by the dopant size effects occurring in substitution sites since the ionic radius of Al^{3+} (0.54 Å) is smaller than Zn^{2+} (0.74 Å) [13, 31].

Moreover, the recorded XRD spectra showed also that the (002) peak position maintains small shift towards higher angle for the Al-Sn co-doping at concentrations of 1% and 0.25% for Al and Sn, respectively. This behavior is expected by considering the dopant size effects in substitution sites since both ionic radii of Sn^{+4} (0.69 Å) and Al^{3+} are smaller than Zn^{2+} [13, 31] (the oxidation states of Al, Sn and Zn elements will be treated later in the XPS analysis).

However, at 0.5%-Sn and for Al-Sn co-doped ZnO thin films (1%-Al), the XRD measurements showed (002) peak shifting towards lower angle which implies an increase in lattice parameters (Tab.2), inducing a volume expansion. In this situation, the change in stress from compressive to tensile cannot be attributed to the dopant size effects. Alternative mechanism contributes to this behavior which is in good agreement with the work of X. Qu *et al.* [32] performed using First-principles calculation. Such volume expansion has been already predicted by the authors for the case of Al-Sn heavily-doped ZnO system which corresponds to our co-doping case of Al concentration of 1% and Sn 0.5% and more. However, the author's explanation remained unclear about the responsible physical mechanism.

On the other hand, J. Zhao *et al*. [33] in their paper stated that the responsible physical mechanism of volume expansion in ZnO lattice lies in repulsive interactions between electrons produced by Al^{3+} and Sn^{4+} when they replace Zn^{2+}. In other words, they justified their simulation results obtained by the free charge effects. The given interpretation of J. Zhao *et al.*, seems to be the most suitable and in agreement with what was already mentioned in literature. Indeed, when high concentrations of donor impurities are incorporated in a semiconductor material, the observed increase in lattice parameters is attributed to two factors: the impurity-size and the electronic effects. The latter results in deformation-potential due to placing free carriers in the conduction band or the valance band [34-37].

In our case it seems that at Sn concentration $\leq 0.25\%$, associated with 1% of Al, the charge effects were weak to be considered as the driving factor in the lattice parameter changes. At Sn concentration ≥ 0.5 %, associated with 1%-Al, the charge effects start to be the dominant factor in the lattice parameters changes.

Furthermore, as clearly shown in Fig. 3, the calculated dislocation density becomes important with the increase of Sn concentration, probably due to Sn occupation of interstitial sites and at the grain boundaries [38-40].

The chemical composition checking by the EDX spectra is given in Fig. 4(a). As expected, EDX spectra show the presence of peaks attributed to zinc and oxygen elements. Fig. 4(b) of AZO samples reveals the presence of zinc, oxygen and aluminium. Furthermore, Fig. 4(c-f) corresponding to ATZO-0.25, ATZO-0.50, ATZO-0.75 and ATZO-1.00 samples show the presence of zinc, oxygen, aluminium and tin. Besides, the presence of silicon on all samples is attributed to the glass substrate. The obtained EDX data confirms the previous XRD analysis.

X-ray photoelectron spectroscopy (XPS) measurement was carried out to investigate the chemical states of elements which compose the thin films. Fig. 5(a) shows the XPS survey spectrum of the sample ATZO-1.00 and reveals the presence of the Zn, O, Al and Sn elements. The Zn 2p, O 1s, Al 2P and Sn 3d high resolution core level XPS spectra are presented in Fig. 5(b–e).

In Fig. 5(b), the Zn 2p spectrum shows two peaks located at 1021.1 and 1044.2 eV with splitting energy (Δ) of 23.1 eV and are assigned as Zn $2p_{3/2}$ and Zn $2p_{1/2}$ respectively of Zn^{2+} in ZnO [41-42].

In Fig. 5(c) the O 1s spectrum can be decomposed into two peaks, the most intense is located at 529.9 eV and assigned to Zn-O bond in wurtzite ZnO structure. The shadow peak at 531.2

eV could be associated with oxygen vacancies in deficient regions within the matrix of ZnO [43] or chemisorbed oxygen impurities [44]. Fig. 5(d) shows the observed Al 2p peak at 73.85 eV, this peak is ascribed to Al^{3+} states [45-48] like in Al_2O_3 compound. The Fig. 5(e) displays the XPS spectrum of Sn 3d. The binding energy of Sn $3d_{5/2}$ peak located at 486.2 eV indicates the Sn^{4+} chemical state which is in good agreement with literature [49-55].

The morphological analysis of the deposited pure ZnO, Al mono-doped ZnO and Al-Sn co-doped thin films was performed by scanning electron microscope (SEM). The micrographs given in Fig. 6 show that the obtained film morphologies depend strongly of the doping concentration. According to Fig. 6, examination of ZnO and ATZO-0.25 samples (Fig. 6(a) and 6(c)) revealed nonmetric spherical grains which are uniformly distributed over the film surface. The average size grain values are 73 nm and 58 nm for ZnO and ATZO-0.25 samples, respectively.

On the other hand, AZO, ATZO-0.50, ATZO-0.75 and ATZO-1.00 sample morphologies (Fig. 6(b), 6(d), 6(e) and 6(f)) indicated granular, dense and homogeneous character. Their average grain size values are 71 nm, 59 nm, 51 nm and 43 nm, respectively.

3.2 Optical properties

The transmittance spectra were measured in the wavelength range 200-2500 nm and depicted in Fig. 7. The deposited film thicknesses have been estimated by fitting the transmittance data Fig. 8 using the spPS technique (seed preprocessing Pattern search) [56]. The obtained values are 291, 220, 240, 306, 303 and 300 nm for ZnO, AZO, ATZO-0.25, ATZO-0.50, ATZO-0.75 and ATZO-1.00 films, respectively. As shown in Fig. 7, the films deposited are highly transparent in the visible range. The average transmittance is about 65% for the un-doped and Al mono-doped ZnO samples and increases with Sn content to reach a value greater than 81% for Al-Sn co-doped ZnO samples. The optical transparency of the obtained ZnO thin films clearly increased with co-doping which means that the dopant atoms are well incorporated in the lattice structure. Fig. 9 shows the surface topography and roughness of ZnO, AZO and ATZO deposited films. The results demonstrate a decreasing RMS roughness values with increasing of Sn concentration, which affects the co-doped films transparency as shown in Fig. 10. This result is in good agreement with literature [31, 57-58].

The optical band gap was determined using the following formula [59]:

$$(ahv)^n = A(hv - Eg) \tag{5}$$

where a is the absorption coefficient, $h\nu$ the photon energy, A, a relation constant and Eg the optical band gap.

We usually take n = 0.5 for indirect band gap semiconductors and n = 2 for direct band gap semiconductors. As ZnO is considered as a direct semiconductor, the optical band gap for each co-doping composition was evaluated by the intersection of the linear portion extrapolation of $(ahv)^2$ versus hv with the photon energy axis (Fig. 11). According to (Fig. 11) the optical band gap increases with dopant concentration from 3.23 eV to 3.30 eV. This gap blue shifting agrees with the literature [60-61] and could be explained by the slight loss of crystallinity and also by the contribution of the Moss–Burstein effect [62-64].

The disorder measure is characterized by Urbach tail. The Urbach energy E_u was estimated by using the following expression [65]:

$$\alpha = \alpha_0 \exp(\frac{h\nu}{E_U}) \quad (6)$$

where α_0 is a constant and E_u the Urbach energy. The E_u evolution for different samples given in Fig.12. shows an increasing in structure disorder with the dopant concentration, in agreement with XRD data and dislocation density curve reported previously. By comparing our results with those of literature [62, 66-67], the E_u variation range reported (92 to 183 meV) correlated with those of the optical band gap, confirms the slight loss of crystallinity.

3.3 Electrical properties

The measured electrical parameters, i.e. conductivity, mobility and carrier concentration of our samples are summarized in Tab. 3. The negative values of carrier concentrations show that as deposited films are n-type. The undoped ZnO samples are characterized by a low conductivity, in agreement with the literature [13, 68]. According to our results, the carrier concentration has been drastically enhanced with aluminium doping, while the mobility remained around the same magnitude. Consequently, the conductivity became 100 times amplified. Moreover, the conductivity of Al-Sn co-doped samples was further improved to reach 0.335 $(\Omega.cm)^{-1}$ value for ATZO-0.75 sample.

One should note that there is a small difference between the conductivity values of ATZO-0.25, ATZO-0.5, ATZO-0.75 and ATZO-1.00 samples (Fig. 13) which means that, in contrast to optical properties, the increasing of Sn concentration has no significant impact on the carrier concentration. This result is consistent with the work of Chien-Yie Tsay et al. [57] in which the authors found a scarcely change in resistivity at low level of Sn-doping (1 to 2%), and a decrease

in carrier concentration due to carrier traps at the grain boundaries, at high level of Sn-doping (over 2%).

4. Conclusion

Thin films of pure, Al mono-doped and Al-Sn co-doped ZnO have been successfully prepared with the spay pyrolysis technique using zinc nitrate, tin chloride and aluminium nitrate as starting chemicals. The structural characterization revealed the high orientation polycrystalline nature of un-doped ZnO films and disoriented polycrystalline nature of the Sn-Al co-doped ZnO. The increasing of the Sn amount at fixed Al concentration showed a slight loss of crystallinity of the ZnO films. The Sn-doping has mainly contributed to improve the transparency of ZnO films while Al-doping has sensibly enhanced the conductivity. The average transmittance and conductivity values (81% and 0.335 $(\Omega.cm)^{-1}$ for the ATZO 1.00 and ATZO 0.75, respectively) obtained by Al-Sn co-doping show an optical and electrical enhancement of spray pyrolysis ZnO thin films obtained from zinc nitrate which are in accordance with the requirements for transparent conducting oxide applications in solar cells [69].

Acknowledgments

The authors would like to acknowledge the financial support of this work by the General Direction of Scientific Research and Technology (DGRSDT/MESRS), Algeria, under CNEPRU project n° A10N01UN220120150004.

References

[1] A. Ouhaibi , M. Ghamnia , M.A. Dahamni , V. Heresanu , C. Fauquet , D. Tonneau , The effect of strontium doping on structural and morphological properties of ZnO nanofilms synthesized by ultrasonic spray pyrolysis method, Journal of Science: Advanced Materials and Devices 3 (2018) 29-36.

[2] Leeseung Kang, Hye Lan An, Ji Young Park, Myung Hwan Hong, Sahn Nahm, Chan Gi Lee, La-doped p-type ZnO nanowire with enhanced piezoelectric performance for flexible nanogenerators, App. Surf. Sci. 475 (2019) 969-973.

[3] Mohd Mubashshir Hasan Farooqi, Rajneesh K. Srivastava, Structural, optical and photoconductivity study of ZnO nanoparticles synthesized by annealing of ZnS nanoparticles, J. Alloy. Compd. (2016). JALCOM 38747.

[4] Ranran Fan, Fei Lu, Kaikai Li, Single-mode channel waveguide at 1540 nm in Er-doped ZnO thin film, J. Lumin. 192 (2017) 410–413.

[5] M. Hjiria, L. El Mir, S.G. Leonardic, A. Pistonec, L. Maviliad, G. Neric, Al-doped ZnO for highly sensitive CO gas sensors, Sensor. Actuat. B-Chem. 196 (2014) 413–420

[6] Yolanda Y. Villanueva, Da-Ren Liu, Pei Tzu Cheng, Pulsed laser deposition of zinc oxide, Thin Solid Films 501 (2006) 366 – 369.

[7] Shalaka C. Navale, I.S. Mulla , Photoluminescence and gas sensing study of nanostructured pure and Sn doped ZnO , Mat. Sci. Eng. C, 29 (2009) 1317–1320.

[8] T.L. Yang, D.H. Zhang, J. Ma, H.L. Ma, Y. Chen , Transparent conducting ZnO:Al films deposited on organic substrates deposited by r.f. magnetron-sputtering , Thin Solid Films 326 (1998) 60–62

[9] Saliha Ilican, Yunus Özdemir, Mujdat Caglar, Yasemin Caglar , Temperature dependence of the optical band gap of sol-gelderived Fe-doped ZnO films , Optik 127 (2016) 8554–8561.

[10] A. Bedia, F.Z. Bedia, M. Aillerie, N. Maloufi, Structural, electrical and optical properties of Al–Sn codoped ZnO transparent conducting layer deposited by spray pyrolysis technique, Superlattices and Microstructures 111 (2017) 714-721.

[11] Emrah Sarica , Vildan Bilgin , Structural, optical, electrical and magnetic studies of ultrasonically sprayed ZnO thin films doped with vanadium , Surf. Coat. Tech. 286 (2016) 1–8.

[12] N. Sadananda Kumar, Kasturi V. Bangera, G.K. Shivakumar , Effect of annealing on the properties of Bi doped ZnO thin films grown by spray pyrolysis technique , Superlattices and Microstructures 75 (2014) 303–310.

[13] A. Nakrela, N. Benramdane, A. Bouzidi, Z. Kebbab, M. Medles, C. Mathieu, Site location of Al-dopant in ZnO lattice by exploiting the structural and optical characterisation of ZnO:Al thin films, Results in Phys. 6 (2016) 133-138.

[14] Rina Pandey, Shavkat Yuldashev, Hai Dong Nguyen, Hee Chang Jeon, Tae Won Kang, Fabrication of aluminium doped zinc oxide (AZO) transparent conductive oxide by ultrasonic spray pyrolysis, Curr. Appl. Phys. 12 (2012) 56-58.

[15] A R Babar, P R Deshamukh, R J Deokate, D Haranath, C H Bhosale and K Y Rajpure , Gallium doping in transparent conductive ZnO thin films prepared by chemical spray pyrolysis , J. Phys. D: Appl. Phys. 41 (2008) 135404.

[16] S. Edinger , N. Bansal, M. Bauch1, R. A. Wibowo, G. U´ jva´ ri1, R. Hamid, G. Trimmel and T. Dimopoulos , Highly transparent and conductive indium-doped zinc oxide films deposited at low substrate temperature by spray pyrolysis from water-based solutions , J. Mater. Sci. 52 (2017) 8591–8602.

[17] C.M. Muiva, T.S. Sathiaraj, K. Maabong, Effect of doping concentration on the properties of aluminium doped zinc oxide thin films prepared by spray pyrolysis for transparent electrode applications, Ceramics International 37 (2011) 555-560.

[18] Preetam Singh, Ajay Kaushal, Davinder Kaur, Mn-doped ZnO nanocrystalline thin films prepared by ultrasonic spray pyrolysis, J. Alloy. Compd. 471 (2009) 11–15.

[19] Murat Tomakin, Structural and optical properties of ZnO and Al-doped ZnO microrods obtained by spray pyrolysis method using different solvents, Superlattices and Microstructures 51 (2012) 372-380.

[20] O. Bazta, A. Urbieta, J. Piqueras, P. Fernández, M. Addou, J.J. Calvino, A.B. Hungría, Influence of yttrium doping on the structural, morphological and optical properties of nanostructured ZnO thin films grown by spray pyrolysis, Ceramics International, 45 (2018) 6842-6852.

[21] Said Benramachea, Boubaker Benhaoua, Okba Belahessen , The crystalline structure, conductivity and optical properties ofCo-doped ZnO thin films, Optik 125 (2014) 5864–5868.

[22] O. Makuku, F. Mbaiwa, T. S Sathiaraj, Structural, Optical and Electrical properties of low temeperature grown undoped and (Al, Ga) co-doped ZnO thin films by spray pyrolysis, Ceramics International, 42 (2016) 14581-14586.

[23] P.V. Raghavendra, J.S. Bhat, N.G. Deshpande, Enhancement of photoluminescence in Sr doped ZnO thin films prepared by spray pyrolysis, Mat. Sci. Semicon. Proc. 68 (2017) 262–269.

[24] Xudong Meng Wei Zheng Bing Han Shuo Li Junping Cai Fu Yang Jingyu Nan Yanfeng Wang, Optical and electrical properties of H and V co-doped ZnO films sputtered at room temperature, Optik, 128 (2017) 27-303.

[25] V. Ganesh, I.S. Yahia, S. AlFaify, Mohd. Shkir, Sn-doped ZnO nanocrystalline thin films with enhanced linear and nonlinear optical properties for optoelectronic applications, J. Phys. Chem. Solids, 100 (2017) 115-125.

[26] Zhanchang Pan, Pengwei Zhang, Xinlong Tian, Guo Cheng, Yinghao Xie, Huangchu Zhang, Xiangfu Zeng, Chumin Xiao, Guanghui Hu, Zhigang Wei, Properties of fluorine

and tin co-doped ZnO thin films deposited by sol–gel method, J. Alloy. Compd. 576 (2013) 31-37.

[27] M. Humayan Kabir , M. Al amin , M.S. Rahman , M.K.R Khan , Infuence of Al doping on microstructure, morphology, optical and photoluminescence properties of pyrolytic ZnO thin Þlms prepared in an ambient atmosphere , Chinese J. Phys. 56 (2018) 2275-2284.

[28] Muhammad R. Islama, Mukhlasur Rahmana, S.F.U. Farhadb, J. Poddera , Structural, optical and photocatalysis properties of sol–gel deposited Aldoped ZnO thin films , Surfaces and Interfaces 16 (2019) 120–126.

[29] A.R. Landa-Cánovas, J. Santiso, F. Agulló-Rueda, P. Herrero, E. Navarrete-Astorga, E. Ochoa- Martínez, J.R. Ramos-Barrado, M. Gabás . Nanostructural changes upon substitutional Al doping in ZnO sputtered films. Ceramics International 45 (2019) 6319-6327.

[30] Mingyang Wu, Dan Sun, Changlong Tan, Xiaohua Tian and Yuewu Huang, Al-doped ZnO monolayer as a promising transparent electrode material: a first-principles study, Materials 10 (2017) 359-372.

[31] H. Aydin H.M. El-Nasser C. Aydin Ahmed. A. Al-Ghamdi F. Yakuphanoglu, Synthesis and characterization of nanostructured undoped and Sn doped ZnO Thin Films via Sol–Gel Approach, App. Surf. Sci. 350 (2015) 109-114.

[32] Xiurong Qu, Shuchen Lü, Dechang Jia, Sheng Zhou and Qingyu Meng, First-principles study of the electronic structure of Al and Sn co-doping ZnO system, Materials Science in Semiconductor Processing 16 (2013)1057-1062.

[33] Jin Zhao, Qiao Liping, Guo Chen, He Zhili, Liu Lidong and Rong Mei, First-priniciple study of electrical and optical properties of (Al,Sn)co-doped ZnO, Optik 127 (2016) 1988–1992.

[34] M. Leszczyński, E. Litwin-Staszewska and T. Suski, Lattice constant of doped semiconductor, Acta Physica Polonica A 88(1995)837-840.

[35] U. Pietsch and K. Unger, The influence of free carriers on the equilibrium lattice parameter of semiconductor materials, Phys. Stat. Sol (a) 80(1983) 165-172.

[36] Chris G. Van de Walle, Effects of impurities on the lattice parameters of GaN, Physical Rreview B 68 165209 (2003)1-5.

[37] Anderson Janotti, Bharat Jalan, Susanne Stemmer and Chris G. Van de Walle, Effects of doping on the lattice parameter of SrTiO3, Applied Physics Letters 100 262104 (2012) 1-3.

[38] M. arshad javid, M. rafi, ihsan ali, Fayyaz hussain, M. imran, Ali nasir , Synthesis and study of structural properties of Sn doped ZnO nanoparticles , Mater. Science-Poland, 34 (2016) 741-746.

[39] A.Karthick, Dr.G.Umadevi and D.Pradhabhan, structural, optical and antibacterial activity studies of sn doped zno thin films prepared by chemical spray pyrolysis technique, International Journal of Research and Analytical Reviews, 5 (2018) 246-260.

[40] Ehssan S Hassan, Tahseen H Mubarak, Khalid H Abass, Sami S Chiad, Nadir F Habubi Maher H Rahid , Abdulhussain A Khadayeir , Mohamed O Dawod1 andIsmaeel A Al-Baidhany , Structural,Morphological and Optical Characterization of Tin Doped Zinc Oxide Thin Film by (SPT), J. Phys. Conf. Ser.1234 (2019) 012013.

[41] A. Amala Rani, Suhashini Ernest. Structural, Morphological, Optical and Compositional Characterization of Spray deposited Ga doped ZnO thin film for Dye-Sensitized Solar Cell Application. Superlattices and Microstructures.75 (2014). 398-408.

[42] Jie Hua, Fanqin Gao, Zhenting Zhao, Shengbo Sang, Pengwei Li, Wendong Zhang ,Xiongtu Zhou, Yong Chen. Synthesis and characterization of Cobalt-doped ZnO microstructuresfor methane gas sensing. Applied Surface Science. 363 (2016) 181-188.

[43] Xinlong Tian, Zhanchang Pan,n, Huangchu Zhang, Hong Fan, Xiangfu Zeng, Chumin Xiao, Guanghui Hu, Zhigang Wei . Growth and characterization of the Al-doped and Al–S Co-doped ZnO nanostructures. Ceramics International. 39 (2013) 6497-6502.

[44] Zhixiang Ye,Ting Wang, Shuang Wu,Xiaohong Ji,Qinyuan Zhanga . Na-doped ZnO nanorods fabricated by chemical vapor deposition and their optoelectrical properties. Journal of Alloys and Compounds. 690 (2017) 189-194.

[45] Nikša Krstulović, Krešimir Salamon, Ognjen Budimlija, Janez Kovač, Jasna Dasović, Polona Umek, Ivana Capan. Parameters optimization for synthesis of Al-doped ZnO nanoparticles by laser ablation in water. Applied Surface Science. 440 (2018) 916-925.

[46] Li Li, Liang Fang, Xian Ju Zhou, Zi Yi Liu, Liang Zhao, Sha Jiang. X-ray photoelectron spectroscopy study and thermoelectric properties of Al-doped ZnO thin films. J. Electron Spectrosc. Relat. Phenom .173 (2009) 7-11.

[47] H.T. Cao, Z.L. Pei, J. Gong, C. Sun, R.F. Huang, and L.S. Wen. Preparation and characterization of Al and Mn doped ZnO (ZnO: (Al, Mn)) transparent conducting oxide films. Journal of Solid State Chemistry .177 (2004) 1480-1487.

[48] Rongyue Liu, Ying Chen, Shuyu Ding, Yuanbo Li, Yong Tian . Preparation of highly transparent conductive aluminum-doped zinc oxidethin films using a low-temperature aqueous solution process for thin-film solar cells applications. sol energ mat sol c. 203 (2019) 110161.

[49] M. Ohtsuka, R. Sergiienko, S. Petrovska, B. Ilkiv, T. Nakamura. Iron-Doped Indium Saving Indium-tin oxide (ITO) Thin Films Sputtered on Preheated Substrates. Optik. 179 (2019) 19-28.

[50] Satirtha K. Sarma, Ratan Mohan, Anupam Shukla. Structural, opto-electronic and photoelectrochemical properties of tin doped hematite nanoparticles for water splitting. Mater Sci Semicond Process. 108 (2020) 104873.

[51] Tiekun Jia , Jian Chen, Zhao Deng, Fang Fu, Junwei Zhao, Xiaofeng Wang, Fei Long. Facile synthesis of Zn-doped SnO2 dendrite-built hierarchical cube-like architectures and their application in lithium storage. Materials Science and Engineering B .189 (2014) 32–37.

[52] T. Potlog, V. Botnariuc, S. Raevschi, M. Dobromir, and D. Luca. XRD and XPS of Cd2SnO4 Thin Films Obtained by Spray Pyrolysis. 3rd International Conference on Nanotechnologies and Biomedical Engineering. IFMBE Proceedings 55. (2016).

[53] Xueli Yang, Sufang Zhang, Qi yu, Liupeng Zhao,Peng Sun, Tianshuang Wang, Fangmeng Liu, Xu Yan, Yuan Gao, Xishuang Liang, Sumei Zhang, Geyu Lu One step synthesis of branched SnO2/ZnO heterostructures and their enhanced gas-sensing properties. Sensors and Actuators B: Chemical. 281 (2019) 415-423.

[54] Zhenyi Zhang, Changlu Shao, Xinghua Li, Li Zhang, Hongmei Xue, Changhua Wang, and Yichun Liu. Electrospun Nanofibers of ZnO-SnO2 Heterojunction with High Photocatalytic Activity. J. Phys. Chem. 114 (2010) 7920-7925.

[55] Zheng Zhang, Zhanhong Yanga,b, Ruijuan Wang, ZhaoBin Feng ,Xiaoe Xie, Qingfeng Liao. Electrochemical performance of ZnO/SnO2composites as anodematerials for Zn/Ni secondary batteries. Electrochimica Acta 134 (2014) 287-292.

[56] R. Miloua, Z. Kebbab, F. Chiker, K. Sahraoui, M. Khadraoui, and N. Benramdane , Determination of layer thickness and optical onstants of thin films by using a modified pattern search method ; Opt. Lett. 37 (2012) 449-451.

[57] Chien-Yie Tsay, Hua-Chi Cheng, Yen-Ting Tung, Wei-Hsing Tuan, Chung-Kwei Lin, Effect of Sn-doped on microstructural and optical properties of ZnO thin films deposited by sol–gel method, Thin Solid Films 517 (2008) 1032-1036.

[58] Konstantin Lovchinov ,Georgi Marinov, Miroslav Petrov, Nikolay Tyutyundzhiev, Tsvetank Babeva. Influence of ZnCl2 concentration on the structural and optical properties of electrochemically deposited nanostructured ZnO. Applied Surface Science. 456 (2018) 69-74.

[59] R. Mimouni, O. Kamoun, A. Yumak, A. Mhamdi, K. Boubaker, P. Petkova, M. Amlouk, Effect of Mn content on structural, optical, opto-thermal and electrical properties of ZnO:Mn sprayed thin films compounds, J. Alloy. Compd. 645 (2015) 100-111.

[60] Mohammad Tajally, Omid Mirzaee, Akbar Eshaghi , The effects of Ti concentration on the structure, optical, and electricalproperties of Al and Ti co-doped ZnO thin films , Optik, 127 (2016) 4645-4649.

[61] N. Chahmat, T. Souier, A. Mokri, M. Bououdina, M.S. Aida, M. Ghers, Structure, Microstructure and Optical Properties of Sn-doped ZnO Thin Films, J. Alloy. Compd. 593 (2014) 148-153.

[62] F.Z. Bedia , A. Bedia, N. Maloufi, M. Aillerie , F. Genty, B. Benyoucef, Effect of tin doping on optical properties of nanostructured ZnO thin films grown by spray pyrolysis technique, J. Alloy. Compd. 616 (2014) 312-318.

[63] Min-I Lee, Mao-Chia Huang, David Legrand, Gilles Lerondel, Jing-Chie Lin, Structure and characterization of Sn, Al co-doped zinc oxide thin films prepared by sol–gel dip-coating process, Thin Solid Films, 570 (2014) 516-526.

[64] N. Rajeswari Yogamalar • A. Chandra Bose , Burstein–Moss shift and room temperature near-band-edge luminescence in lithium-doped zinc oxide , Appl. Phys. A 103 (2011) 33–42.

[65] Said Benramache, Achour Rahal , Boubaker Benhaoua , The effects of solvent nature on spray-deposited ZnO thin filmprepared from Zn (CH3COO)2, 2H2O , Optik 125 (2014) 663– 666.

[66] Charles Moditswe Cosmas M. Muiva Albert Juma, Highly conductive and transparent Ga-doped ZnO thin films deposited by chemical spray pyrolysis, Optik 127 (2016) 8317-8325.

[67] G. Turgut and E. Sönmez , A Study of Pb-Doping Effect on Structural, Optical, and Morphological Properties of ZnO Thin Films Deposited by Sol–Gel Spin Coating ; Metall. Mater. Trans. A, 45 (2014) 3675-3685.

[68] Kamal Baba, Claudia Lazzaroni, Mehrdad Nikravech, ZnO and Al doped ZnO thin films deposited by spray plasma: Effect of the growth time and Al doping on microstructural, optical and electrical properties, Thin Solid Films 595 (2015) 129-135.

[69] C. Guillén , J. Herrero , TCO/metal/TCO structures for energy and flexible electronics, Thin Solid Films 520 (2011) 1–17.

Figures captions and tables

Figure 1: Schematic diagram of the Spay Pyrolysis system used.

Figure 2: (a) XRD patterns of pure ZnO, AZO and ATZO samples, (b) Magnified and higher solution XRD pattern.

Figure 3: Grain size, strain and dislocation density evolutions of ZnO, AZO and ATZO samples.

Figure 4: Energy dispersive X-ray (EDX) spectra of the obtained films. (a) ZnO, (b) AZO, (c) ATZO-0.25, (d) ATZO-0.50, (e) ATZO-0.75 and (f) ATZO-1.00.

Figure 5: (a) XPS full survey scan of ATZO-1.00 thin films, (b) XPS peaks of Zn 2p, (c) XPS peak of O 1s. (d) XPS peak of Al 2p and (e) XPS peak of Sn 3d.

Figure 6: SEM images of the obtained films (a) ZnO, (b) AZO, (c) ATZO-0.25, (d) ATZO-0.50, (e) ATZO-0.75 and (f) ATZO-1.00.

Figure 7: Transmittance spectra of the obtained films.

Figure 8: Measured and fitted transmittance data as a function of wavelength (sample ZnO).

Figure 9: Surface topologies of the obtained films (sample dimensions 800 μm × 800 μm) (a) ZnO, (b) AZO , (c) ATZO-0.25, (d) ATZO-0.50, (e) ATZO-0.75 and (f) ATZO-1.00.

Figure 10: Transmittance at wavelength 550 nm versus RMS.

Figure 11: Variation of $(\alpha hv)^2$ versus energy of the obtained films.

Figure 12: Band gap and Urbach energy of ZnO, AZO and ATZO samples.

Figure 13: Conductivity evolution of ZnO, AZO and ATZO samples.

Table 1: Samples designations and spayed solution compositions.

Table 2: Structural parameters of pure, Al-doped and Al-Sn co-doped ZnO.

Table 3: Electrical parameters of ZnO, AZO and ATZO samples at room temperature.

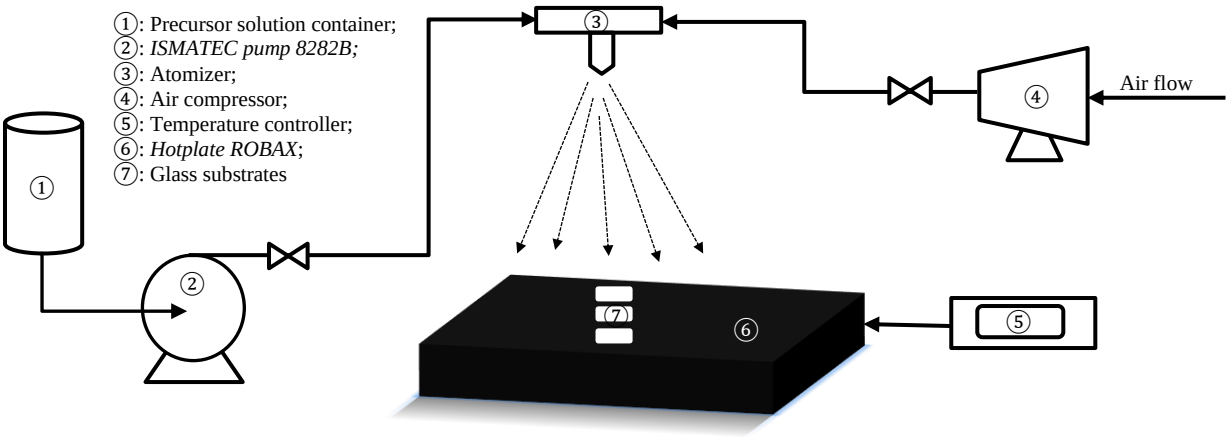
①: Precursor solution container;
②: ISMATEC pump 8282B;
③: Atomizer;
④: Air compressor;
⑤: Temperature controller;
⑥: Hotplate ROBAX;
⑦: Glass substrates
Air flow

Figure 1

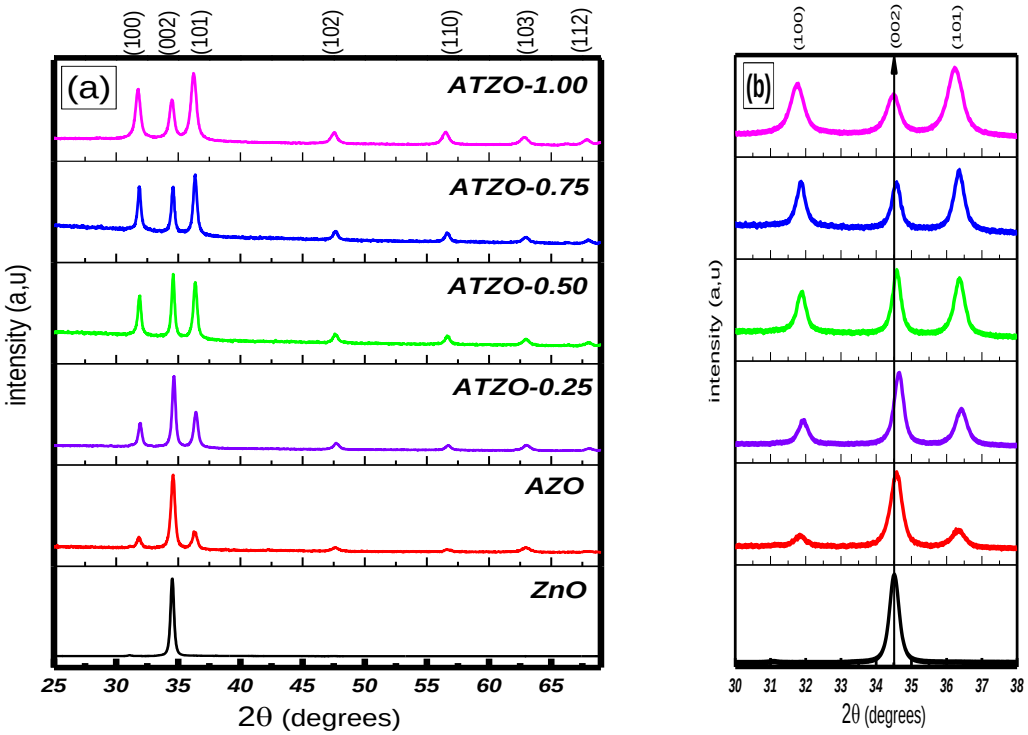
(100)
(002)
(101)
(102)
(110)
(103)
(112)
(a)
ATZO-1.00
ATZO-0.75
ATZO-0.50
ATZO-0.25
AZO
ZnO
intensity (a,u)
25 30 35 40 45 50 55 60 65
2θ (degrees)
(100)
(002)
(101)
(b)
intensity (a,u)
30 31 32 33 34 35 36 37 38
2θ (degrees)

Figure 2

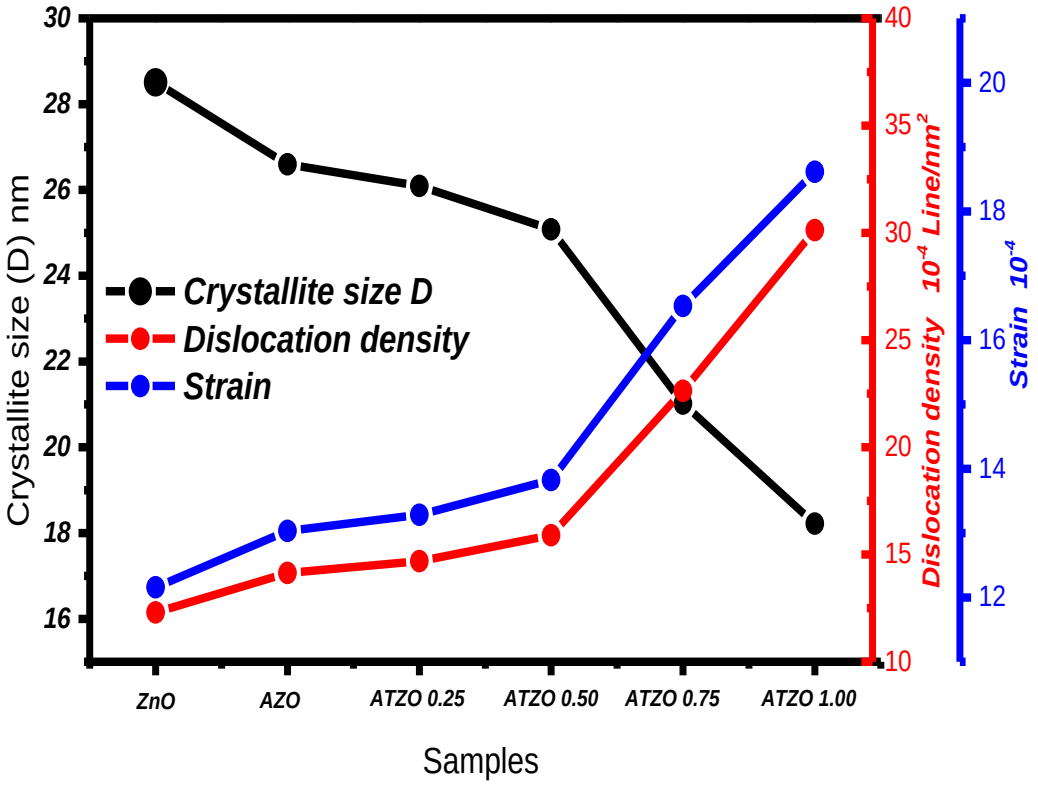
Crystallite size (D) nm
Dislocation density 10⁻⁴ Line/nm²
Strain 10⁻⁴
Crystallite size D
Dislocation density
Strain
ZnO
AZO
ATZO 0.25
ATZO 0.50
ATZO 0.75
ATZO 1.00
Samples

Figure 3

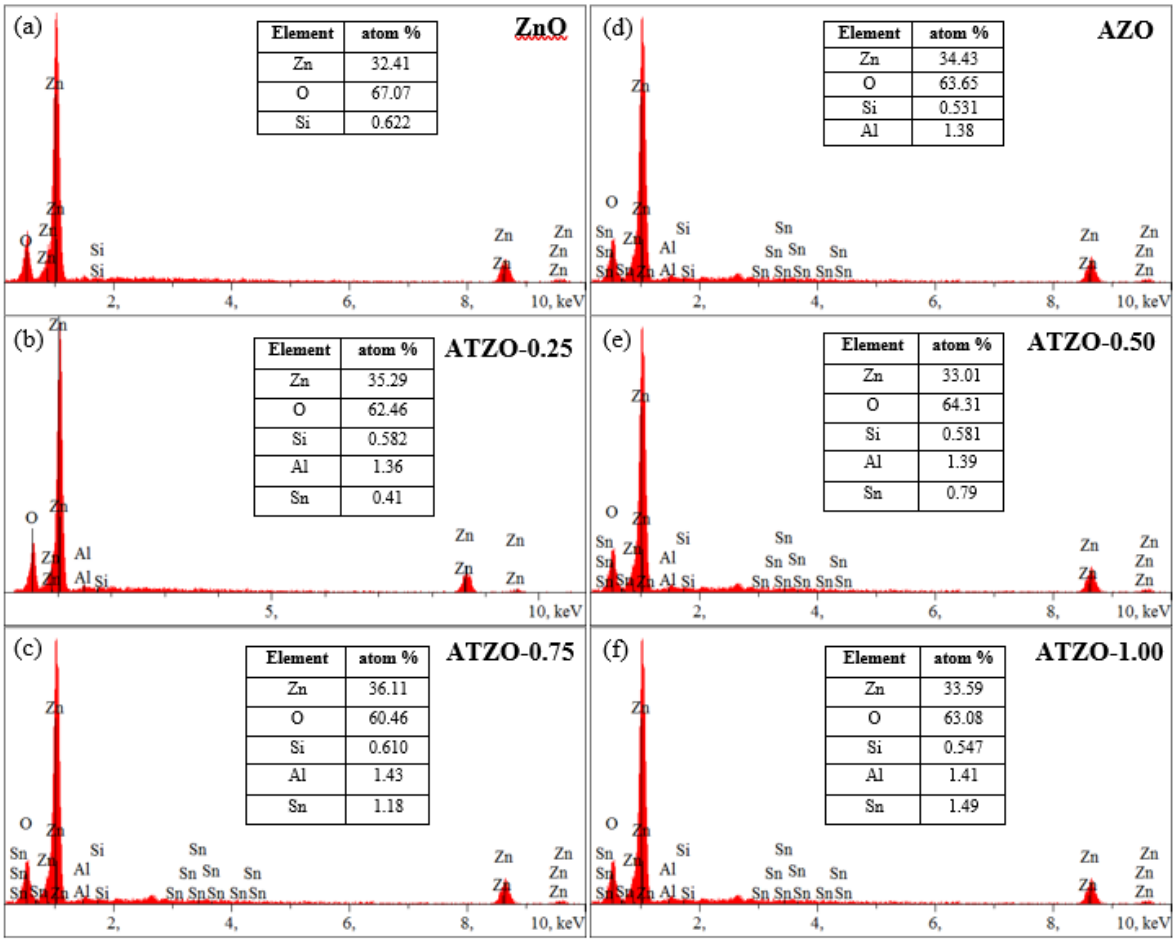
(a)
ZnO
Element | atom %
Zn | 32.41
O | 67.07
Si | 0.622
(d)
AZO
Element | atom %
Zn | 34.43
O | 63.65
Si | 0.531
Al | 1.38
(b)
ATZO-0.25
Element | atom %
Zn | 35.29
O | 62.46
Si | 0.582
Al | 1.36
Sn | 0.41
(e)
ATZO-0.50
Element | atom %
Zn | 33.01
O | 64.31
Si | 0.581
Al | 1.39
Sn | 0.79
(c)
ATZO-0.75
Element | atom %
Zn | 36.11
O | 60.46
Si | 0.610
Al | 1.43
Sn | 1.18
(f)
ATZO-1.00
Element | atom %
Zn | 33.59
O | 63.08
Si | 0.547
Al | 1.41
Sn | 1.49
2, 4, 6, 8, 10, keV
5, 10, keV

Figure 4

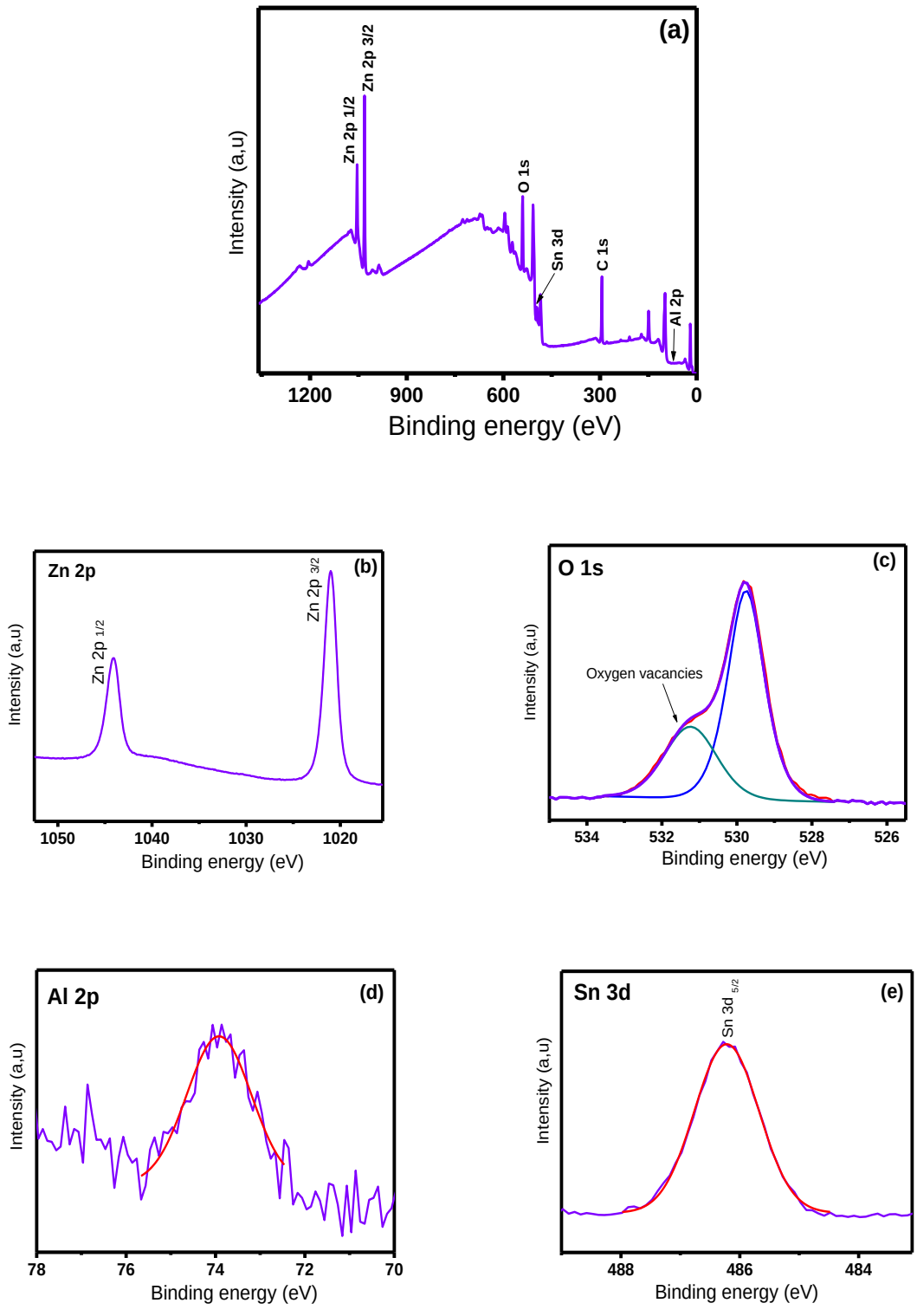
(a)
Zn 2p 3/2
Zn 2p 1/2
O 1s
Sn 3d
C 1s
Al 2p
Intensity (a,u)
1200
900
600
300
0
Binding energy (eV)
Zn 2p
(b)
Zn 2p 1/2
Zn 2p 3/2
Intensity (a,u)
1050
1040
1030
1020
Binding energy (eV)
O 1s
(c)
Oxygen vacancies
Intensity (a,u)
534
532
530
528
526
Binding energy (eV)
Al 2p
(d)
Intensity (a,u)
78
76
74
72
70
Binding energy (eV)
Sn 3d
(e)
Sn 3d 5/2
Intensity (a,u)
488
486
484
Binding energy (eV)

Figure 5

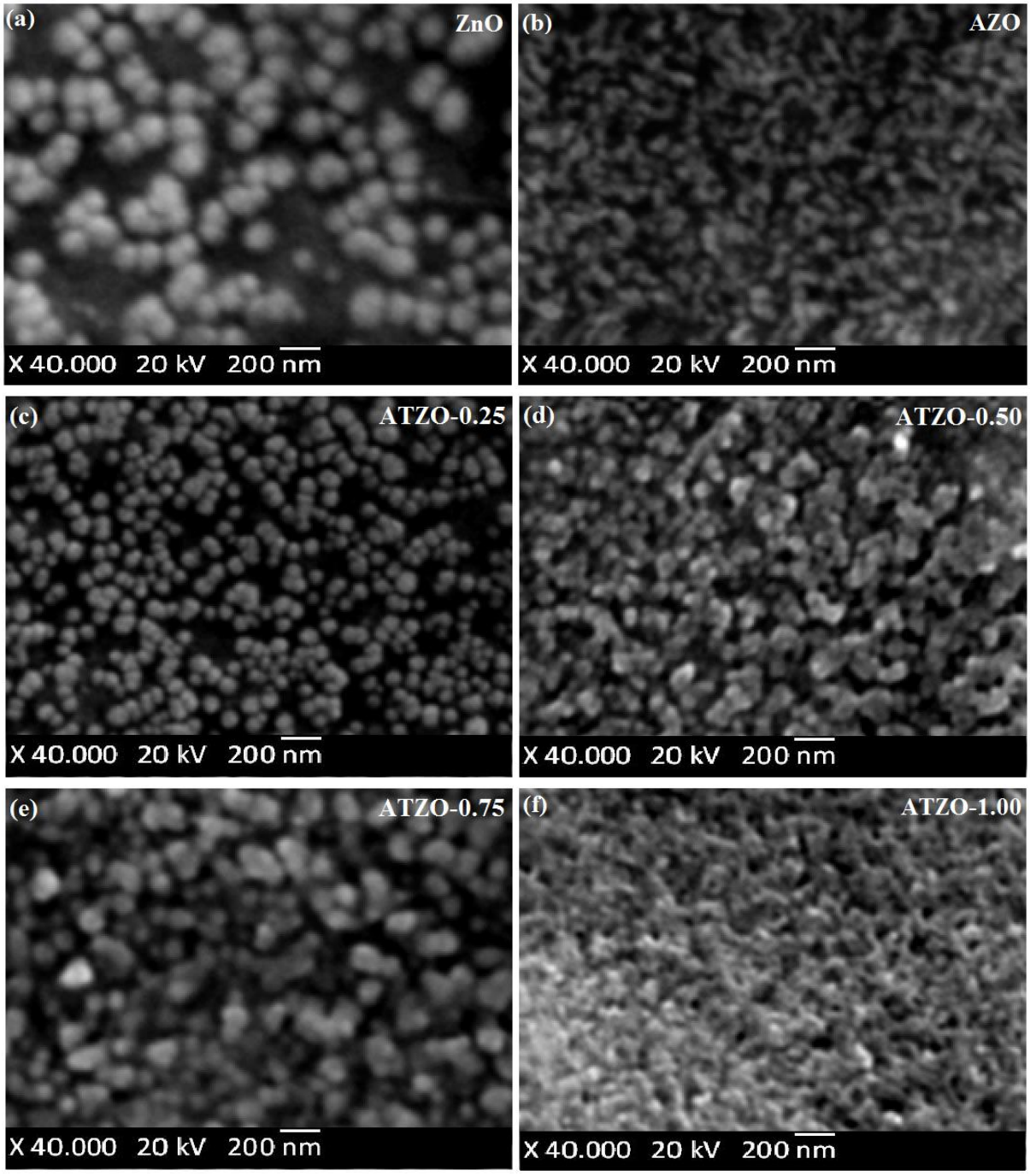
(a)
ZnO
X 40.000 20 kV 200 nm
(b)
AZO
X 40.000 20 kV 200 nm
(c)
ATZO-0.25
X 40.000 20 kV 200 nm
(d)
ATZO-0.50
X 40.000 20 kV 200 nm
(e)
ATZO-0.75
X 40.000 20 kV 200 nm
(f)
ATZO-1.00
X 40.000 20 kV 200 nm

Figure 6

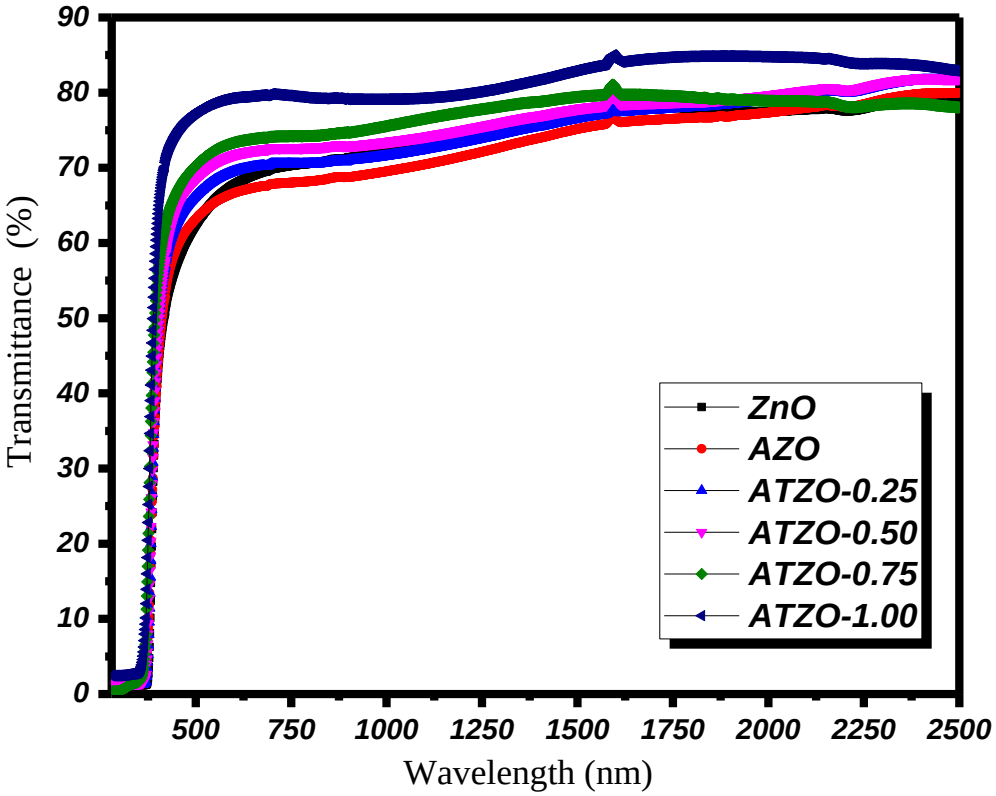
Transmittance (%)
90
80
70
60
50
40
30
20
10
0
500
750
1000
1250
1500
1750
2000
2250
2500
Wavelength (nm)
ZnO
AZO
ATZO-0.25
ATZO-0.50
ATZO-0.75
ATZO-1.00

Figure 7

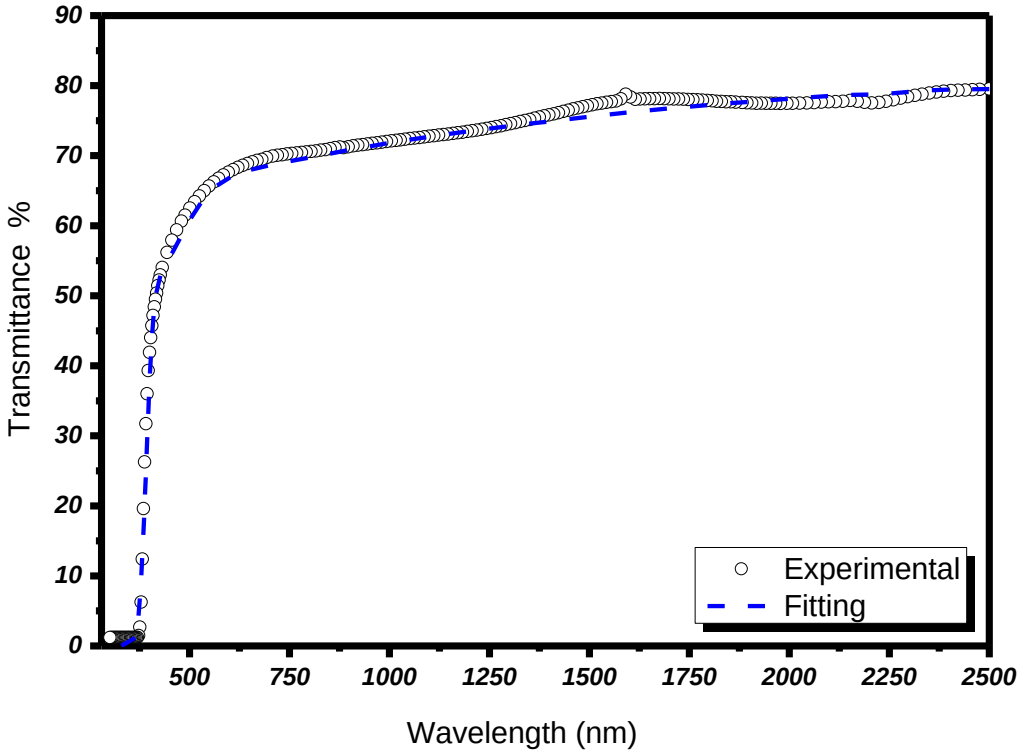
Transmittance %
Wavelength (nm)
Experimental
Fitting
0
10
20
30
40
50
60
70
80
90
500
750
1000
1250
1500
1750
2000
2250
2500

Figure 8

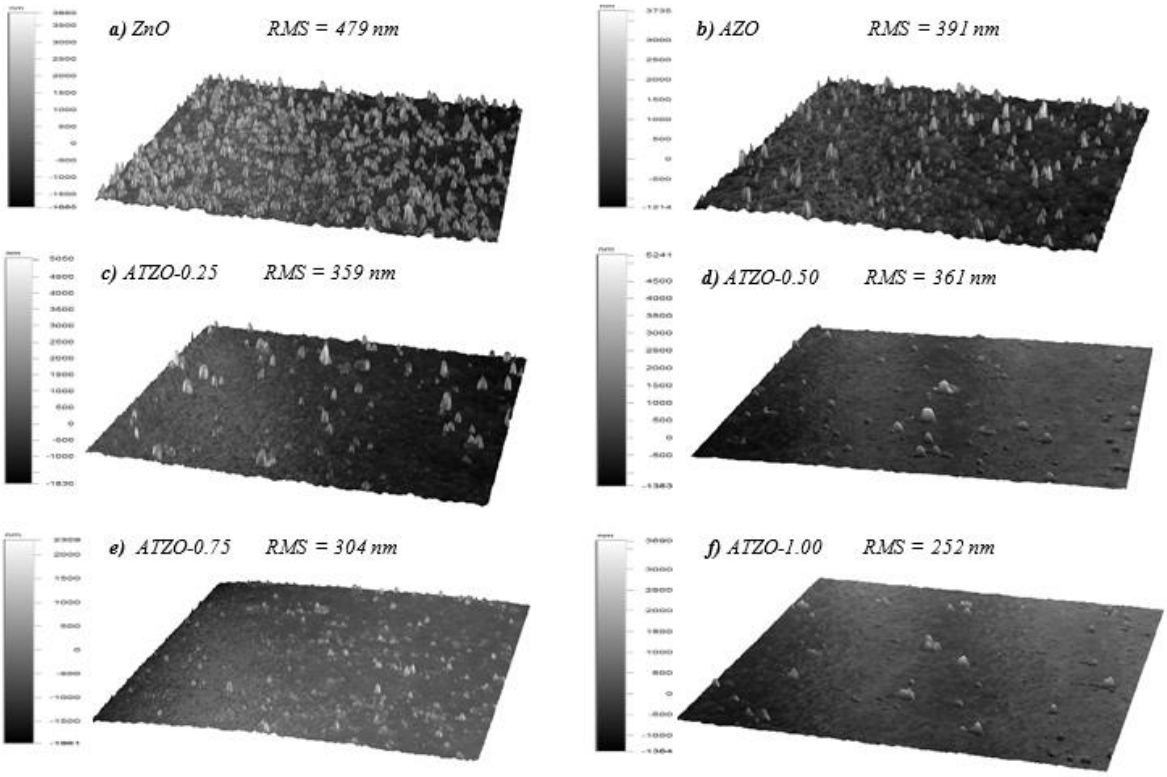
a) ZnO RMS = 479 nm
b) AZO RMS = 391 nm
c) ATZO-0.25 RMS = 359 nm
d) ATZO-0.50 RMS = 361 nm
e) ATZO-0.75 RMS = 304 nm
f) ATZO-1.00 RMS = 252 nm

Figure 9

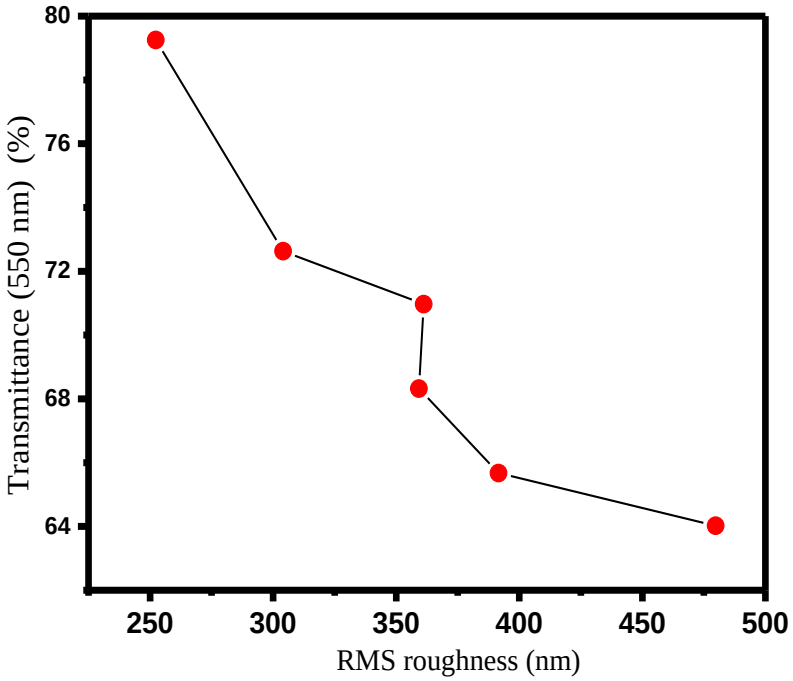
80
76
72
68
64
Transmittance (550 nm) (%)
250
300
350
400
450
500
RMS roughness (nm)

Figure 10

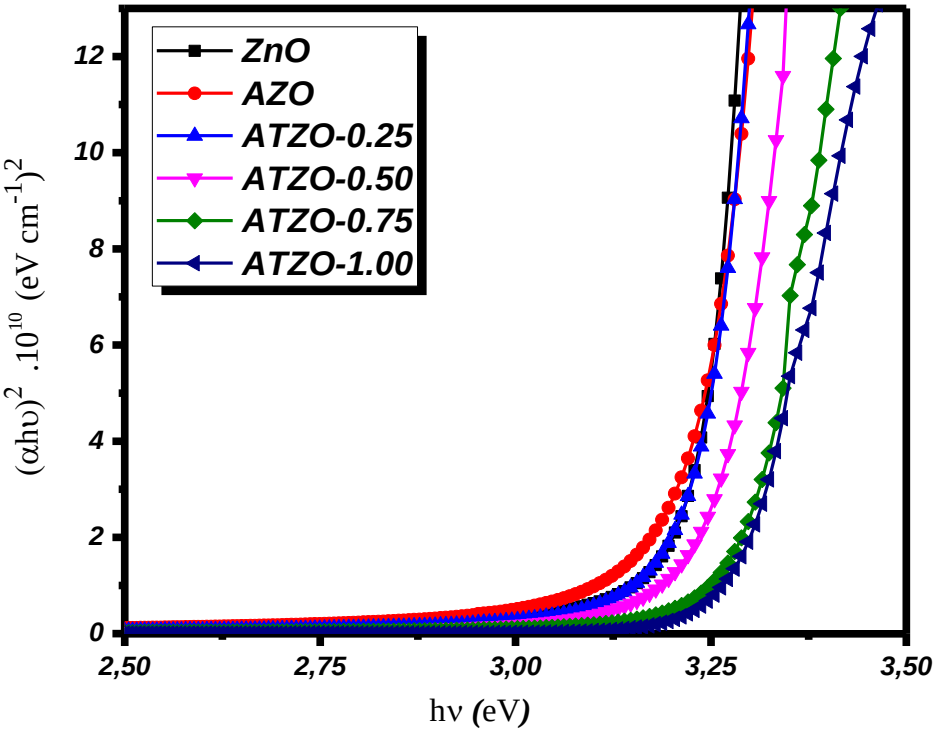
ZnO
AZO
ATZO-0.25
ATZO-0.50
ATZO-0.75
ATZO-1.00
12
10
8
6
4
2
0
2,50
2,75
3,00
3,25
3,50
(αhυ)2 .10^10 (eV cm-1)2
hν (eV)

Figure 11

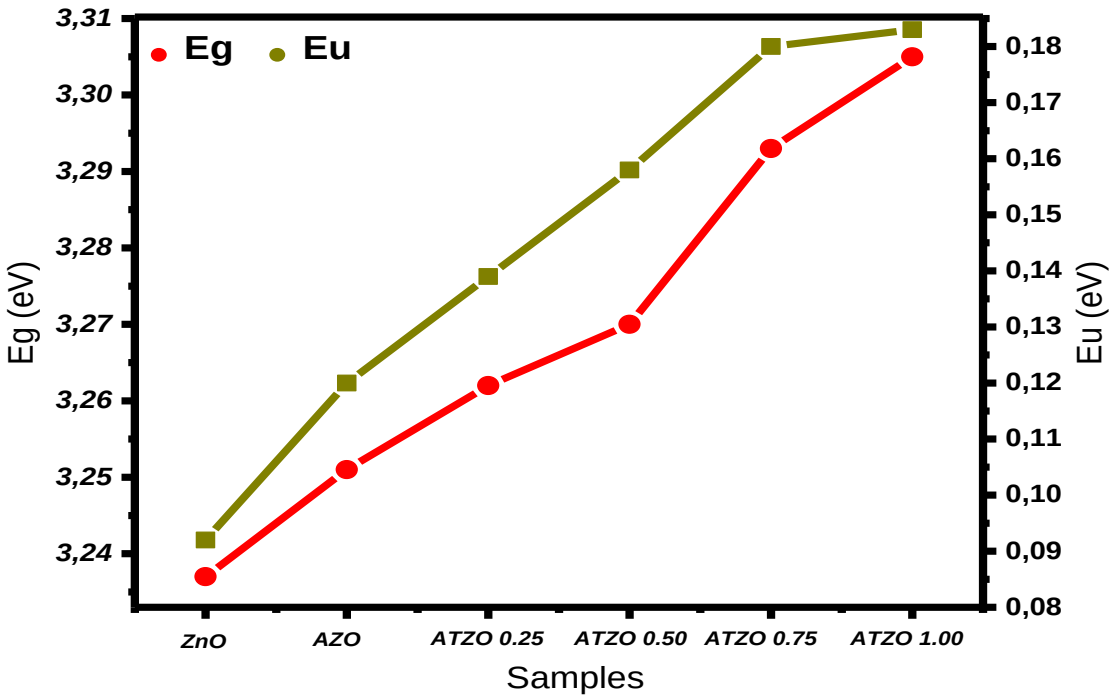
Eg
Eu
3,31
3,30
3,29
3,28
3,27
3,26
3,25
3,24
Eg (eV)
0,18
0,17
0,16
0,15
0,14
0,13
0,12
0,11
0,10
0,09
0,08
Eu (eV)
ZnO
AZO
ATZO 0.25
ATZO 0.50
ATZO 0.75
ATZO 1.00
Samples

Figure 12

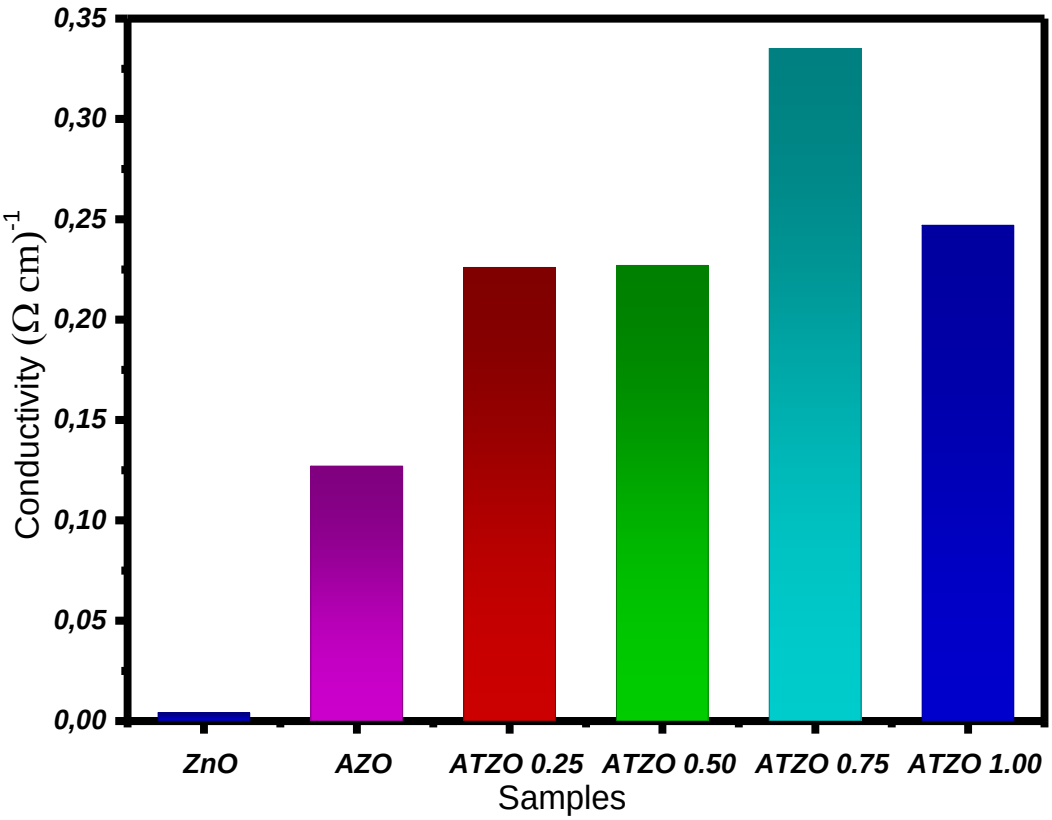
0,35
0,30
0,25
0,20
0,15
0,10
0,05
0,00
Conductivity (Ω cm)-1
ZnO
AZO
ATZO 0.25
ATZO 0.50
ATZO 0.75
ATZO 1.00
Samples

Figure 13

Table 1

Designations	Samples	Sprayed solution compositions
Pure ZnO (undoped)	ZnO	100 % dissolved $Zn(NO_3)_2$
Al doped ZnO	AZO	99 % dissolved $Zn(NO_3)_2$ + 1% dissolved $Al(NO_3)_3$
Al-Sn co-doped ZnO	ATZO-0.25	98.75% dissolved $Zn(NO_3)_2$ + 1% dissolved $Al(NO_3)_3$ + 0.25% dissolved $SnCl_2$
Al-Sn co-doped ZnO	ATZO-0.50	98,5% dissolved $Zn(NO_3)_2$ + 1% dissolved $Al(NO_3)_3$ + 0.5 % dissolved $SnCl_2$
Al-Sn co-doped ZnO	ATZO-0.75	98.25% dissolved $Zn(NO_3)_2$ + 1% dissolved $Al(NO_3)_3$ + 0.75% dissolved $SnCl_2$
Al-Sn co-doped ZnO	ATZO-1.00	98% dissolved $Zn(NO_3)_2$ + 1% dissolved $Al(NO_3)_3$ + 1% dissolved $SnCl_2$

Table 2

Samples	$2\theta^0$ (002)	FWHM $.10^{-3}$ (Degrees)	Crystallite size (nm)	a (A^0)	c (A^0)	Strain (10^{-4})	Dislocation density (10^{-4} Line/nm^2)
ZnO	34.521	5.093	28.508	3.241	5.192	12.157	12.300
AZO	34.574	5.460	26.595	3.240	5.184	13.033	14.138
ATZO-0.25	34.620	5.564	26.094	3.238	5.181	13.283	14.686
ATZO-0.50	34.583	5.791	25.080	3.239	5.183	13.824	15.898
ATZO-0.75	34.569	6.925	21.020	3.242	5.184	16.530	22.632
ATZO-1.00	34.530	7.797	18.218	3.243	5.190	18.614	30.129

Table 3

Samples	Mobility (cm^2/V_S)	Carrier Concentrations (cm^{-3})	conductivity $(\Omega .cm)^{-1}$
ZnO	$4.30.10^{-01}$	$-5.91.10^{+16}$	$4.06.10^{-03}$
AZO	$3.14.10^{-01}$	$-2.54.10^{+18}$	$1.27.10^{-01}$
ATZO-0.25	$7.00.10^{-01}$	$-2.02.10^{+18}$	$2.26.10^{-01}$
ATZO-0.50	$23.3.10^{-01}$	$-0.61.10^{+18}$	$2.27.10^{-01}$
ATZO-0.75	$2.28.10^{-01}$	$-9.19.10^{+18}$	$3.35.10^{-01}$
ATZO-1.00	$3.40.10^{-01}$	$-4.54.10^{+18}$	$2.46.10^{-01}$